JOURNAL OF MATERIALS SCIENCE **39** (2004) 7259–7267

A simple transient numerical model for heat transfer and shape evolution during the production of rings by centrifugal spray deposition

R. M. WARD, M. D. BARRATT, M. H. JACOBS, Z. ZHANG, A. L. DOWSON
IRC in Materials Processing, University of Birmingham, Birmingham, B15 2TT, UK
E-mail: r.m.ward@bham.ac.uk

Centrifugal spray deposition, the atomisation of a liquid metal by centrifugal force and the subsequent collection of the atomised droplets on a reciprocating collector, is currently being developed for the production of high performance Fe, Ni and Ti based ring-shaped components for use in aerospace and gas turbine containment applications. The process combines the technical, economic and metallurgical benefits of more conventional gas-assisted spray forming techniques with the advantage that it can easily operate under vacuum, reducing potential problems from gas entrapment and thermally induced porosity. In order to aid process development, understanding and optimisation, a transient numerical heat and mass transfer model has been developed that is capable of predicting the evolution of the deposit temperature distribution during spraying. The model has been validated experimentally using thermocouple measurements obtained during the production of 35 kg (340 mm diameter) IN718 rings and qualitative correlations have been observed between the predicted data and the type/distribution of porosity and second phase precipitates in the deposit. The model is currently being further developed and integrated with droplet size distribution and cooling models to provide a better insight into the physics and operational parameters which control deposit shape and microstructure.

1. Introduction

Centrifugal Spray Deposition (CSD) converts liquid metal into a near net-shaped preform via centrifugal atomisation and deposition, and offers unique opportunities for producing both powders and axi-symmetric ring shaped components, for example for use in aerospace and gas turbine containment applications.

Metal is melted in a crucible and poured through a nozzle onto a rapidly rotating disk. At the edge of the disk it is atomised to form a spray that travels outwards onto a substrate where it solidifies to form a fine-grained solid deposit. The process combines the cost and metallurgical benefits of conventional gas assisted spray forming operations with the additional advantage that the process can operate under vacuum or reduced pressure. Thus the costs of gas delivery, storage and recycling are reduced, and potential metallurgical problems deriving from gas entrapment are virtually eliminated. More details are available in [1]. Rings of IN718 have been succesfully produced by CSD (Fig. 1) and ring-rolled to produce properties equivalent to those achieved by conventional routes [2].

Whilst considerable effort has been directed worldwide at modelling spray forming, much of the focus has been on gas-assisted deposition techniques such as Osprey^{TM}. A good fundamental understanding of gas-assisted deposition processes has evolved from this (e.g. [3–5]), and droplet based deposition models have started to emerge linking microstructure to the state of the spray at the point of impact [6]. Less attention has been directed at the CSD process, and where work has been undertaken it has tended to be concentrated on the atomisation process itself and on understanding the liquid metal flow on the disc up to the point of atomisation. The principal aim of the current modelling work was to extend these studies so as to provide a predictive tool which would aid process understanding, and facilitate the selection and optimisation of the key operational parameters which influence microstructure and shape evolution during deposition. On this basis it was decided to focus mainly on the macroscopic and thermal aspects of deposition, recognising that (subject to slight modifications) droplet cooling and impact models developed for the Osprey process are becoming increasingly well established and transferable, and that work on modelling the fluid dynamic aspects of centrifugal atomisation is continuing elsewhere.

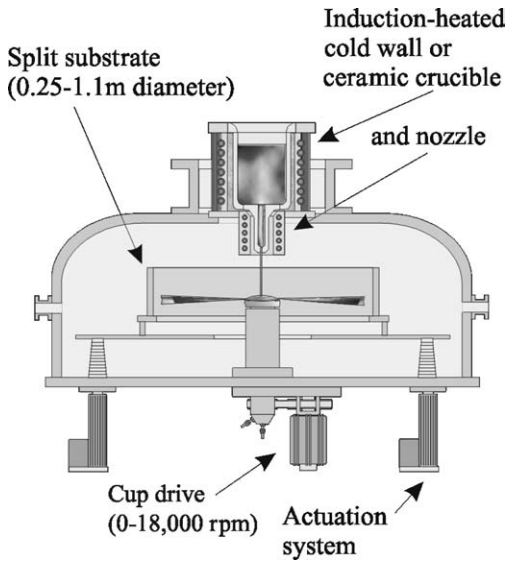

Figure 1 The CSD process.

2. Aspects of centrifugal spray deposition

If a solid deposit is produced, its structure and shape are controlled by a number of inter-related parameters. The product quality can be viewed as being ultimately dependent on: deposit temperature history on a macroscale; droplet splatting, solidification and consolidation; deposit shape history; and the properties of the material being sprayed. Factors that link these together include the spray/substrate motion and the cooling of the deposit, and it is useful to examine these relationships in more detail.

2.1. Spray/substrate motion

For given *average* rates of deposition of mass and enthalpy, a number of choices for substrate or spray motion are possible:

1. *No reciprocation*. The substrate or spray moves continuously in one direction. At the point of deposition, the additions of mass and enthalpy are locally high. A given region in the deposit is unlikely to be remelted once it has solidified.
2. *Some reciprocation*. The spray reciprocates relative to the substrate, so that a given point in the deposit undergoes repeated heating and cooling. The local addition of mass and enthalpy is not as high as in (1), but macroscopic regions of the deposit may be remelted as fresh layers of spray are deposited.
3. *Very fast reciprocation*. The relative reciprocation of the spray and substrate is rapid enough that a given point in the deposit does not (except at the droplet scale) undergo repeated heating and cooling. The local rates of addition of mass and enthalpy now equal the average rates.

In practice, both options 1 and 3 present particular challenges. In option 1, the deposit would be produced with a significant axial temperature gradient, possibly leading to problems of shrinkage or distortion as spraying and subsequent cooling progressed. Option 3 is difficult to achieve practically because of the high forces which would be necessary to rapidly accelerate the substrate. In the experimental work to be presented here, a reciprocating pattern of substrate motion relative to the spray was used so that the deposit was built up from 30 layers of spray droplets.

TABLE I Deposition conditions during CSD of IN718 ring

Deposit thickness (mm)	Thickness per pass (mm)	Thermocouples?	Macro sample?
14	0.47		√
17	0.57	Substrate	
22	0.73		√
34	1.13	Deposit	√

2.2. Deposit cooling

Particularly when CSD is undertaken at low pressure, the predominant heat loss from the deposit occurs through different mechanisms to those in conventional gas-assisted spray deposition. As convective cooling plays less of a role under vacuum, radiation to the surroundings and conduction to the substrate become relatively more important for cooling the deposit. Deposit cooling can be considered in terms of a feedback path which includes the current shape of the deposit and its contact with the substrate, the history of its shape and temperature, the development of stress and strain, and the efficiency of droplet sticking. The effects of this complexity may compromise the accuracy of simple models, and this will be discussed later.

3. Experimental and numerical details

A ring of IN718 encompassing four spraying conditions will be considered in this paper, consisting of 30 layers of material (spray passes) each taking 11.5 s (345 s total spraying time) as shown in Table I.

The ring was produced with a slight variation in its thickness as function of angle around the centreline. This was achieved by pouring the stream of liquid metal onto the cup slightly away from its axis of rotation, shown in Fig. 2, producing a spray with a slight azimuthal variation in its mass flux.

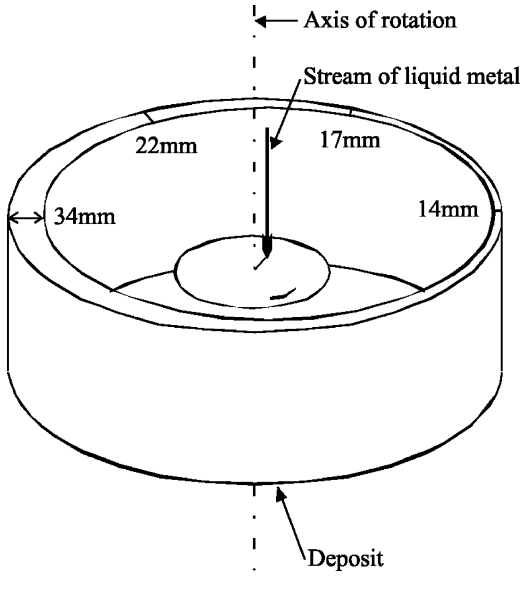

Figure 2 Production of samples.

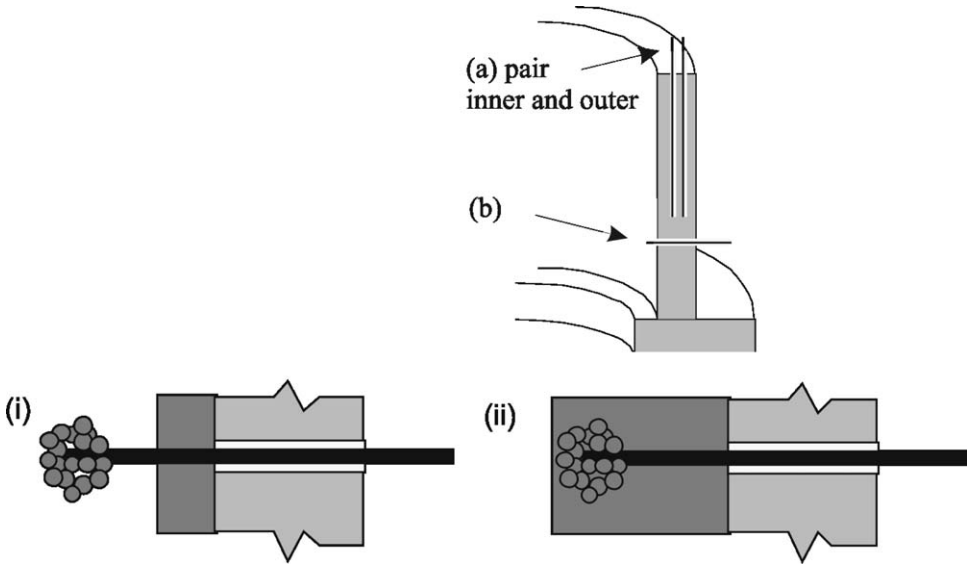

Figure 3 Thermocouple placement.

While the authors accept that this could have also lead to azimuthal variations in particle size distribution and residence time on the disk (and hence spray temperature), it was thought to be the best way of producing a consistent set of experimental samples with as many other important process variables kept constant.

The temperature of the liquid metal in the melting crucible was monitored using a two-colour pyrometer, subsequently calibrated against dip thermocouple readings. However the temperature of the spray itself (in free flight, after leaving the cup) was not measured, due to the physical difficulty in doing so. However based on the measured liquid temperature, a spray temperature of 1450°C was used in this simulation.

Thermocouples were mounted in the substrate in pairs as shown in Fig. 3a at a number of heights in a region where the deposit was 17 mm thick. Two were also mounted through the substrate as shown in Fig. 3b so as to protrude into the deposit (initially into empty space) in a region of 34 mm deposit thickness. However it was observed that spray particles deposited on their tips before the deposit surface had reached them. This caused the thermocouples to read a high temperature unexpectedly early in the experiment, as shown in Fig. 3(i), and may have lead to slight errors later on, as shown in Fig. 3(ii). Samples were cut from the deposit at locations at which the deposit thicknesses were 14, 22 and 34 mm.

The amount of material deposited per pass can in principle be estimated a-priori from the estimated spray parameters and the substrate dimensions and motion, but in these examples it was calculated after the experiments from the measured deposit thickness and the known number of spray passes occurring.

As discussed previously the heat transfer between the deposit and the substrate was represented by a heat transfer coefficient (HTC), dependent on the temperature of the deposit outer surface (next to the substrate). Values were initially chosen based on experience from casting and plasma melting [7] and other authors' investigations [6], and these were then iteratively refined.

A 2d transient numerical approach was used in the model to account for experimentally observed axial variations in microstructure, edge effects, and heat flow in both the axial and radial directions, and also to provide predictive capability for modelling the substrate motion necessary for producing deposits with internal and external shape. It is recognised that the heat flow will in reality have been 3 dimensional, due to the azimuthal variation in the deposit thickness, however by inspection of the thermocouple readings and model predictions (admittedly a somewhat circular argument) the azimuthal temperature gradient was likely to have been below 4°C/cm. Due to the vertical reciprocation of the spray, however, the vertical temperature gradient near the point of spray deposition was likely to have been around 50–100°C/cm, and the radial gradient over 100°C/cm. Fluid flow was deliberately not modelled, on the basis that for effective control of the deposition process solidification must be confined to a relatively thin mushy layer at the surface of the deposit (in order to avoid slumping), and that the onset of fluid flow can be predicted from temperature. The spray was also modelled as discrete blocks of material at a single temperature, rather than a population of droplets with individual sizes and temperatures; again this was to simplify the model computationally, because of the emphasis on macroscopic phenomena. A finite-volume heat-transfer approach was adopted, using as a basis the standard partial differential equation (PDE) for transient heat flow analysis:

$$\rho_{\mathrm{d}} C_{\mathrm{p}}(T) \frac{\partial T}{\partial t} = \nabla(K(T)\nabla T) \qquad (1)$$

ρ_{d} = density; C_{p} = specific heat capacity; T = temperature; t = time; K = thermal conductivity.

Heat transfer was assumed to involve conduction (axial and radial) within the deposit and substrate, and radiative losses from the deposit to the substrate and

chamber walls, and from the substrate to the chamber. Grey body radiative exchange was assumed between the deposit (emissivity = 0.27) and substrate (emissivity = 0.45), with view factors of 1.

The complexity of the cooling of the deposit by the substrate mentioned previously was handled by a simple approximation. A temperature dependent heat transfer coefficient (HTC) was used as the interface between the deposit and the substrate, to account for the varying contact conditions as the rear surface of the deposit cools and contracts away from the substrate. In reality the nature of the contact between these two surfaces is complex and will be influenced by a number of factors including the thermal history and associated temperature dependent property variations (elastic modulus, thermal expansion coefficient, flow stress) in the substrate and the deposit, and the development of temperature and transformation induced residual stresses. To properly accommodate these effects would have required a much more computationally intensive model, and in this case it was assumed that the temperature dependent heat transfer coefficient would give reasonable approximations. The validity of this assumption can be checked by comparing the model predictions with experimental results under a range of operating conditions.

Temperature dependent material properties (density, thermal conductivity and enthalpy) were used for the mild steel collector and the deposit [8]. Phase transitions were accounted for by including their latent heat into a modified specific heat capacity over appropriate temperature ranges. Owing to the additional computational complexity, non-equilibrium thermal properties were not used in this simple simulation, although it is recognised that they would be relevant because of the fairly short solidification times investigated here. Following [8] it was also chosen to consider that 100% fraction solid was present above the Laves phase temperature, so the solidus temperature was taken as 1260°C [also 9]; the implications of the choice of solidus temperature are discussed later. The PDE was discretised on the chosen geometry with explicit boundary conditions into a set of nonlinear ordinary differential equations which were solved using Matlab's ODE15S to predict temperature as a function of time. Using a 1.2 GHz PC it was possible to simulate the spray forming process at between 0.25 and 4× real time depending on how finely the spray was represented. Once spray was no longer being added to the mesh, because deposition had finished, much quicker simulation was possible—of the order of 100 to 1000× faster than real time. Further information of the construction of the model and example simulations is available from http://www.irc.bham.ac.uk/theme1/atomisation/research.htm.

4. Comparison of model predictions with experimental results

The model was used to predict the temperature distribution in the deposit as a function of time. Thermocouple measurements will be presented first in Fig. 4, and compared with the predicted temperatures in Fig. 5.

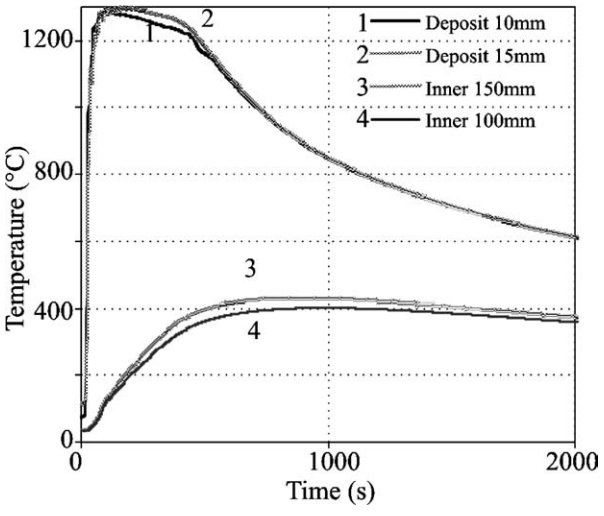

Figure 4 Measured temperatures in the substrate and deposit.

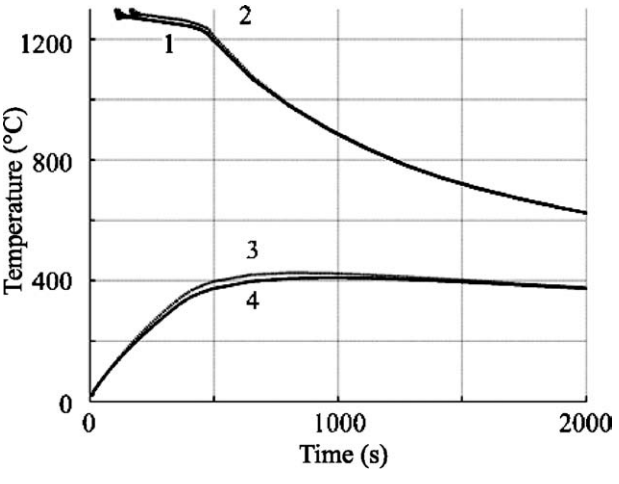

Figure 5 Predicted temperatures in the substrate and deposit.

Sample macrostructures are also presented and discussed along with predictions of local solidification time, surface temperature during spraying, time of final solidification and of remelting.

With reference to Fig. 4, for curves labelled 'inner' in the legend, the subsequent number represents the distance from the top of the substrate to the measurement point. For curves labelled 'deposit' the subsequent number represents the depth of penetration of the thermcouple into the deposit. It should be noted that, as discussed previously, the thermocouples in the deposit registered a high temperature before the bulk of the deposit had reached them.

As the simulation assumes measurements by perfect 'virtual' thermocouples, there is no buildup of spray particles on their tips in the deposit. Hence the deposit temperature histories only start at the time when the deposit reaches their tip locations. This is the reason that the two highest temperature curves in Fig. 5 do not start at 0 s, but rather at the times that the deposit reaches 10 and 15 mm thickness.

A direct comparison between the model predictions and the measured values is shown in Fig. 6. Slight differences (up to approximately 50°C) can be seen between the measured and predicted deposit temperatures after spraying has finished, possibly suggesting that the

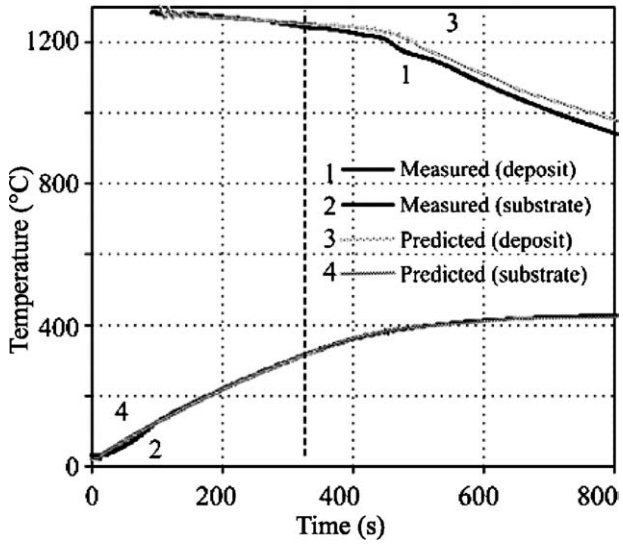

Figure 6 Temperatures in the deposit (>600°C) and substrate (<600°C). Predicted (pale/patterned line) and measured (solid line). The approximate time at which spraying finished is shown by the vertical line.

HTC's have underestimated the changes in the contact conditions as the deposit contracts away from the substrate during cooling.

Samples were taken from deposits produced at 0.47, 0.73 and 1.13 mm per spray pass. The samples were prepared using a Struers Plano 220 grinding disc and were then fine polished using Struers MD cloths and 9 μm to 1 μm diamond suspensions. After optical microscopy in the as-polished condition the samples were then immersion etched in Kallings No. 2 reagent.

Typical images are shown in Fig. 7. The material produced at 0.47 mm/pass (7a) can be seen to contain fairly coarse porosity, likely to have been produced during the splatting of spray droplets. The material produced at 0.73 mm per pass (7b) shows comparatively little porosity (and that which is present should be vacuum-filled). The material produced at 1.13 mm per pass, however, shows a high level of porosity (7c) (likely to have been created by solidification shrinkage) and Laves phase (7d). Although not shown here, there was significant radial and axial variation in the distribution of this porosity within the deposit produced at 1.1 mm/pass. Most of the porosity was found in approximately the middle 75% of the deposit's height, from the surface down to 50–60% of the depth towards the substrate.

A post processor was then used on the predicted time-temperature data to estimate important solidification parameters such as local solidification time (LST) etc., to better understand the development of the macrostructures shown above. The distribution of predicted local solidification times in the deposit under different spraying conditions will be considered first, and these are

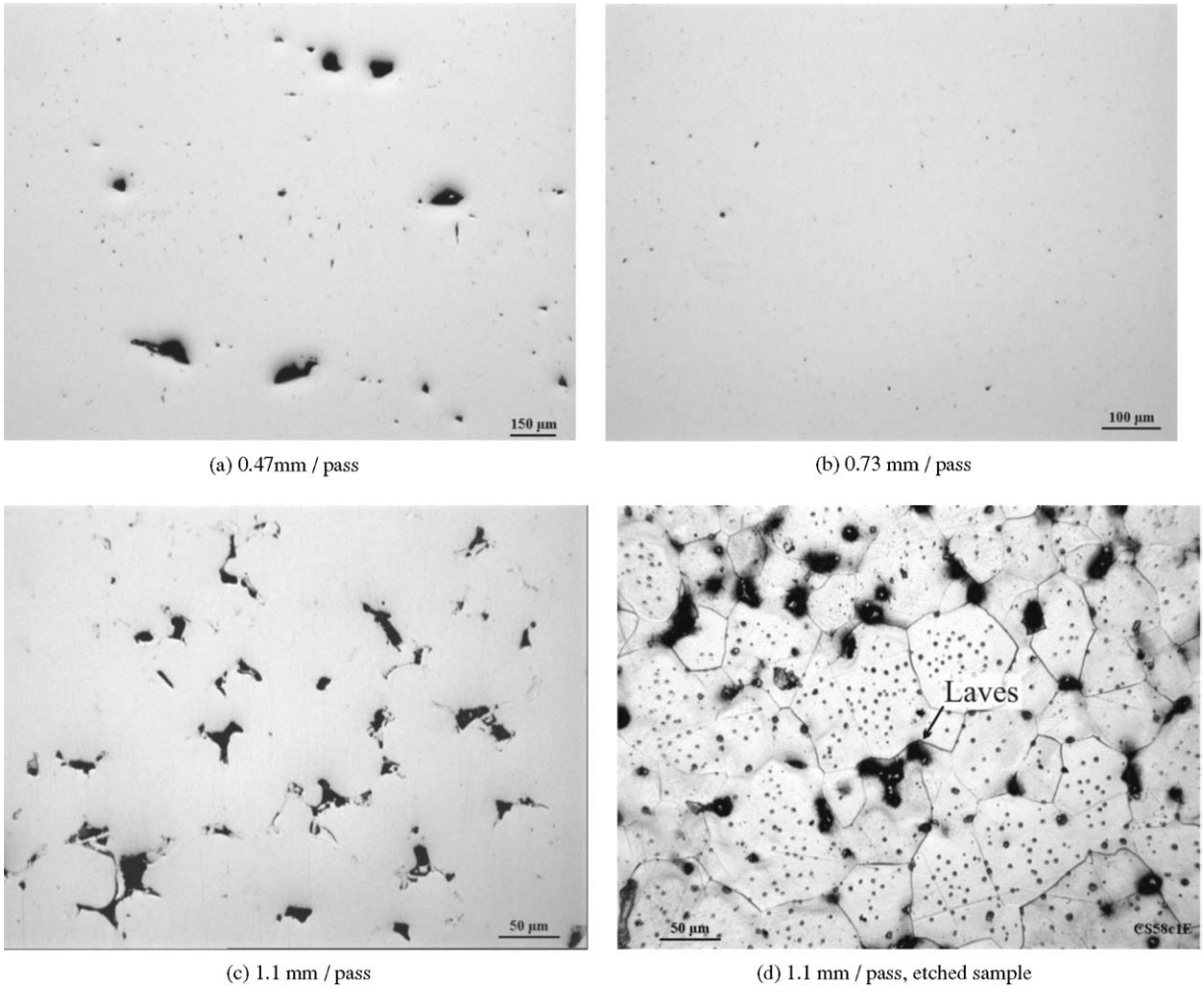

(a) 0.47mm / pass

(b) 0.73 mm / pass

(c) 1.1 mm / pass

(d) 1.1 mm / pass, etched sample

Figure 7 Sample microstructures from deposits produced under different conditions: (a) 0.47 mm/pass, (b) 0.73 mm/pass, (c) 1.1 mm/pass, and (d) 1.1 mm/pass, etched sample.

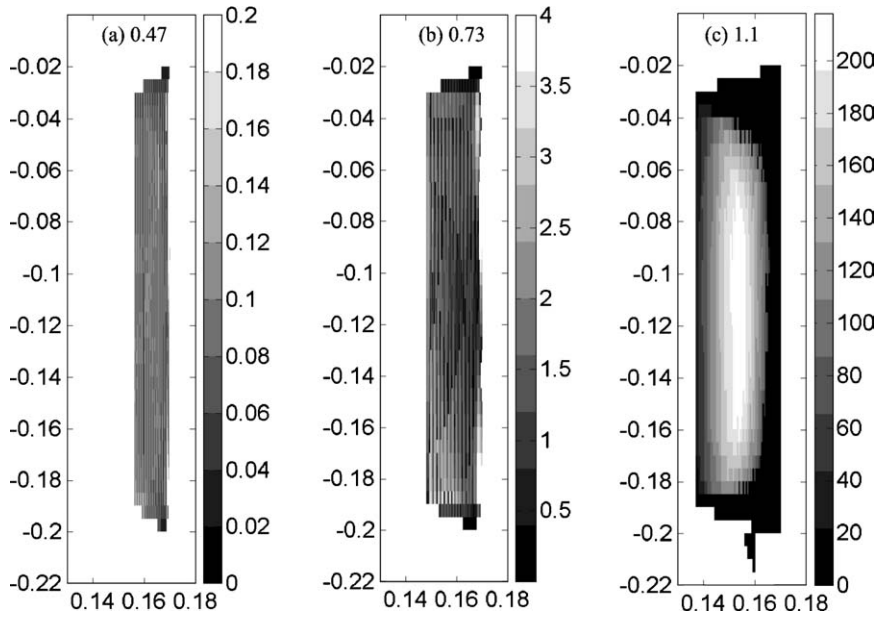

Figure 8 Local solidification time for samples produced at 0.47, 0.73 and 1.13 mm per spray pass respectively. The grey scale on each plot indicates time in seconds. The horizontal and vertical axes on each plot indicate distance in m. On the vertical axis, −0.02 m is at the top of the deposit, and −0.20 m is at the bottom. On the horizontal axis, the centre of the axisymmetric geometry is at 0 m, and the deposit outer surface is at 0.17 m.

presented in Fig. 8. In each case the deposition conditions presented are, from left to right, 0.47, 0.73 and 1.13 mm per spray pass respectively, and the grey value at a given point in the deposit indicates its LST according to the scale on the right.

A number of vertical lines can be seen in the predicted maps of LST values—these are due to the reciprocation of the spray over the substrate (or rather of the substrate against the spray). The LST of fresh spray hitting the deposit will be affected by the time interval since material was last deposited there. At the top and bottom of the deposit's height, the spray will hit twice in quick succession due to the reciprocation, followed by a long time interval. At the middle of the deposit's height, the spray will hit with evenly spaced intervals. It is important to note that the predicted *last* LST values are shown here. Due to the reciprocation it is possible that some points may be remelted as the next layer of spray is deposited on them (see Fig. 11). Fig. 8 shows the LST for the last solidification (i.e., the last time while between the solidus and liquidus temperatures) of a given point.

For deposition at 0.47 mm/pass, the predicted local solidification times are short (typically <100 ms). Even though these predictions must be treated as rough approximations, given the porosity found in the deposit produced under these conditions, this may suggest that arriving spray droplets did not have sufficient time to flow and completely fill any voids before solidification. For deposition at 0.73 mm/pass, solidification times in the order of 1–3 s are typically predicted, varying in radial bands (as at 0.47 mm/pass) due to the substrate motion described previously. For deposition at 1.13 mm/pass, however, very different solidification conditions are predicted. In this case times of over 200 s are predicted in some areas with the following results:

- phases different from those found in the two previous spraying conditions may form (e.g., approximately 1% vol. fraction Laves phase was found in 718 samples solidified with an LST of approximately 200 s in [10])
- there may be significant flow of mushy material during solidification leading to shrinkage porosity

It can also be seen that at 1.13 mm/pass the local solidification times now form a much smoother distribution radially, indicating that the deposit is no longer solidifying completely in discrete layers but rather as a continuous process.

Close inspection of Fig. 8 shows that for deposits produced at 0.47 and 0.73 mm/pass the predicted LST values of the first few layers are somewhat higher than for further layers. As stated previously, the HTC values used include mechanical effects such as the slight shrinkage of the deposit away from the substrate that is believed to occur as spraying proceeds in this geometry (a ring-shaped component inside a substrate). The HTC values should therefore be time-varying, but in the interests of simplicity this model uses best-fit time-averaged values. This may have had an effect when predicting the temperature history of the first few layers of material to hit the substrate, as the HTC may in reality have been initially higher before there had been any contraction. This effect would become less important as spraying progressed, and indeed the model predictions of temperatures in the substrate and deposit are fairly accurate.

The temperature of the surface of the deposit onto which fresh spray arrives was also predicted throughout the deposition process, as surface temperature will strongly influence the dynamics of splatting and cooling experienced by spray droplets on impact. In Fig. 9, the grey value at a given point in deposit gives the temperature at the time at which fresh spray was deposited onto it, according to the scale on the right.

The surface temperature of the material produced at 0.47 mm/pass is predicted to be approximately 140°C below the alloy solidus, so droplets that impinge on it

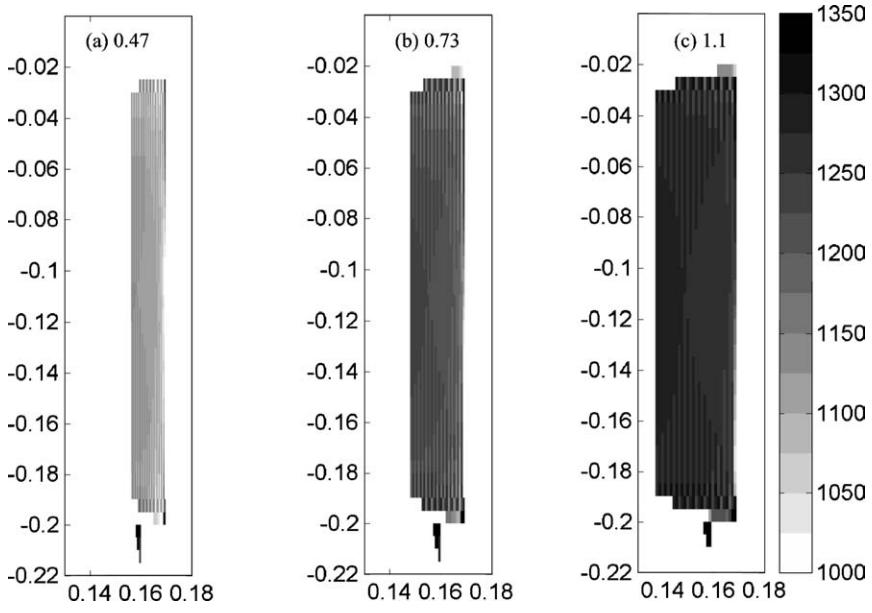

Figure 9 Temperature of material onto which fresh spray arrives, for deposits produced at 0.47, 0.73 and 1.13 mm per spray pass respectively. The grey scale indicates temperature in degrees centigrade. The horizontal and vertical axes indicate distance in m.

will solidify quickly, leading to porosity. The surface temperature at 0.73 mm/pass is predicted to be approximately 30–50°C below the solidus, allowing more time for spray droplets to fill holes before solidification. The surface surface temperature at 1.13 mm/pass is however predicted to be approximately halfway between the solidus and liquidus. This would allow droplets to flow more on impact, but would also allow the deposit as a whole to flow due to solidification shrinkage and gravity. Evidence of flow in the whole deposit can be seen in Fig. 7: the sample of 1.13 mm/pass material from the bottom of the deposit (Fig. 9b) is thicker than that from the middle (Fig. 9a). For the material produced at the other deposition rates, however, the bottom and mid-height thicknesses are approximately equal.

The observation that the least amount of porosity was produced when the surface temperature was initially approximately 40°C below the solidus temperature might, at first sight, conflict with [3] in which it was argued that the best conditions were when the deposit surface and the spray droplets were both mushy. However in the experiments modelled here, as the spray moves successive droplets will be deposited onto a surface that has already been heated by the droplets deposited momentarily before. In this case although the temperature of the surface before spraying was *initially* e.g., 40°C below the solidus, this will rise rapidly as the spray passes so that a percentage of the spray will impact onto a surface *above* the solidus.

Predictions of the time for final solidification throughout the deposit (i.e., the time at which a given point solidifies for the last time, if there is any remelting during spraying) for the different spraying conditions are shown in Fig. 10, below. Material produced at both

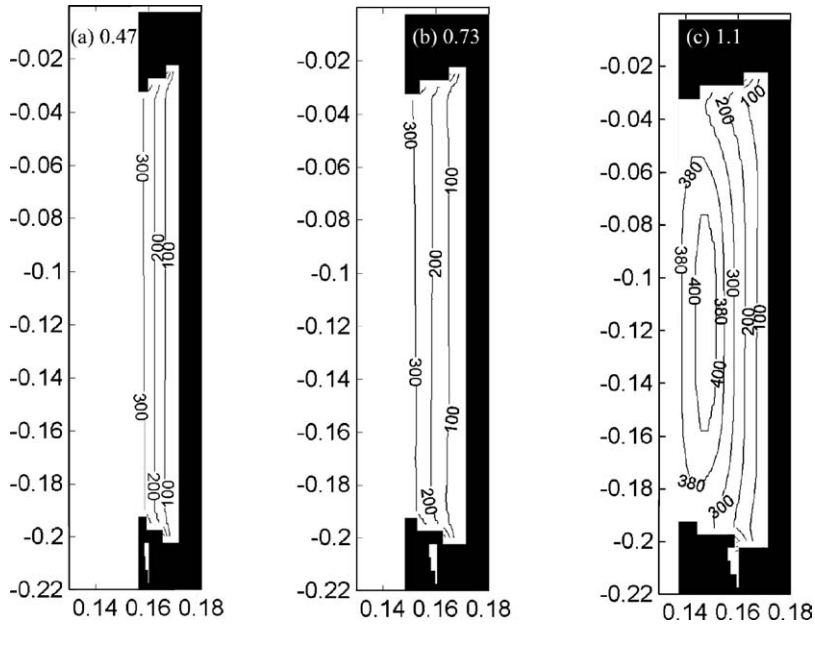

Figure 10 The predicted times of final solidification throughout the deposit, as produced at 0.47, 0.73 and 1.13 mm per spray pass respectively. The contours indicate time in seconds. The horizontal and vertical axes indicate distance in m.

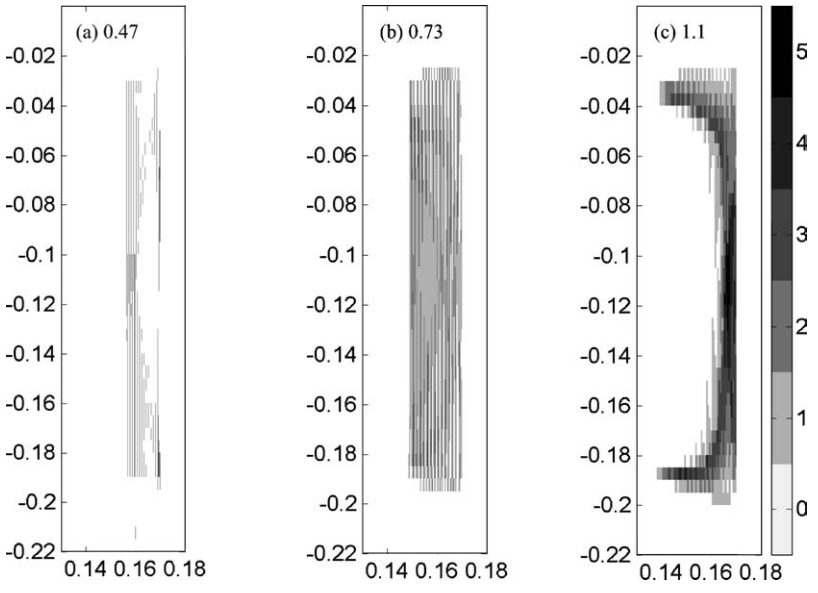

Figure 11 The predicted number of times that a given point will be remelted during deposition, at 0.47, 0.73 and 1.13 mm per spray pass respectively. The grey values indicate number of remelts. The horizontal and vertical axes indicate distance in m.

0.47 and 0.73 mm/pass is predicted to solidify incrementally from the outer face of the ring towards the inner face as spraying progresses. The material produced at 1.13 mm/pass, however, is predicted to solidify not in layers but more as a whole, like a traditional casting, and significant axial variation is also predicted. The material predicted to solidify last (indicated by the '400s' contour in Fig. 10c) is below the deposit surface by approximately one third of the total thickness, which can lead to the formation of shrinkage porosity. Reasonable qualitative agreement was observed between the region of material predicted to solidify almost last (e.g., the '380s' contour in Fig. 10c) and the areas of greatest shrinkage porosity in the deposit.

Finally, the model was also used to predict the number of times that a given point in the deposit would be remelted during deposition as shown in Fig. 11.

It is interesting to note that under deposition at 0.47 mm/pass most of the material is not predicted to remelt once it has been sprayed. This might mean that the fresh spray is unable to satisfactorily bond to it, hence leading to porosity. In the main, the material produced at 1.1 mm/pass is also not predicted to remelt, but in this case it is because it stays mushy throughout most of the spraying time (i.e., it does not ever fully solidify until spraying has finished, leading to problems of shrinkage porosity as described previously). Most of the material produced at 0.73 mm/pass, however, is predicted to remelt once. (In fact a fine-scaled pattern of zero, single and double remelting is predicted, but the average over a couple of layers of elements is close to 1). It is possible that the limited remelting of the surface as spray arrives will allow the spray to satisfactorily bond to the surface, without leading to significant shrinkage porosity. This corresponds qualitatively with experimental observations—the material produced at 0.73 mm/pass in Fig. 7 shows the lowest porosity.

As a note, when considering these predicted estimates of solidification parameters it must be remembered that the results are sensitive to the solidus and liquidus temperatures used. From the literature it can be found that different values for the INCONEL 718 solidus and liquidus temperatures have been used by different organisations, and at different times. In this study the solidus temperature did not affect the calculation of predicted temperatures, as temperature dependent (equilibrium) properties were used for enthalpy, density and thermal conductivity throughout; instead the solidus temperature was only used in the subsequent analysis of the predicted temperatures to derive LST, time of final solidification, and number of times remelted. Nonetheless for example the predicted local solidification times are sensitive to the exact solidus temperature used; reducing the solidus temperature value from 1260 to 1250°C was found to increase the maximum LST in Fig. 8c from approximately 220 to 250 s.

Despite the approximations inherent in the model, it has proved to be helpful for designing experiments, and for analysing the measurements obtained. It should also be helpful to aid research into scaling the process to industrial sizes.

5. Conclusions

The numerical heat flow model predicted deposit temperature distributions during CSD close to those measured experimentally, and was useful in understanding the development of macro- and micro-structure. The model prediction of the onset of non-incremental solidification was consistent with the observation of significant shrinkage porosity and Laves Phase. The lowest porosity was produced under conditions in which the surface temperature of the growing deposit was predicted to be approximately 30–50°C below the alloy solidus, and in which the material was remelted once during deposition.

A useful addition to the model would be to include stress/strain during solidification, to allow predictions of the transient deposit shape. This would reduce the

reliance on experimentally determined boundary conditions, but at the cost of greater complexity and computational requirements.

Acknowledgements

This work was supported by the EPSRC (GR/M74399/01), Doncasters Ltd., Rolls-Royce PLC, and QinetiQ. Many thanks to M. P. Glynn for experimental and practical work.

References

1. A. L. DOWSON, M. H. JACOBS and M. D. BARRATT, in PM2Tech 2001, New Orleans, May 2001, (Metal Powder Indutries Federation, Princeton, NJ, 2001) p. 3153.
2. M. D. BARRATT, M. H. JACOBS and A. L. DOWSON, in PM2Tech 2001, May 2001 (Metal Powder Indutries Federation, Princeton, NJ, 2001) p. 3168.
3. P. MATHUR, S. ANNAVARAPU, D. APELIAN and A. LAWLEY, *Mater. Sci. and Eng.* A **A142** (1991) 261.
4. G. C. CHU and J. PIEN, in Proceedings of the Julian Szekely Memorial Symposium on Materials Processing, 1997, edited by H. Y. Sohn, J. W. Evans and D. Apelian (TMS, Warrendale, PA, 1997) p. 423.
5. J. S. ZHANG, H. CUI, X. J. DUAN, Z. Q. SUN and G. L. CHEN, *Mater. Sci. and Eng.* A **A267** (2000) 257.
6. Q. XU, V. V. GUPTA and E. J. LAVERNIA, *Acta Mater.* **48** (2000) 835.
7. R. M. LOTHIAN, P. D. LEE, M. MCLEAN, R. M. WARD, T. P. JOHNSON and M. H. JACOBS, in Proceedings of International Symposium on Liquid Metal Processing and Casting, Santa Fe, Feb. 1997, edited by A. Mitchell and P. Auburtin (AVS, 1997) p. 133.
8. P. N. QUESTED, K. C. MILLS, R. F. BROOKS, A. P. DAY, R. TAYLOR and H. SZELAGOWSKI, in Proceedings of International Symposium on Liquid Metal Processing and Casting, Santa Fe, Feb. 1997, edited by A. Mitchell and P. Auburtin (AVS, 1997) p. 1.
9. http://asm.matweb.com/search/SpecificMaterial.asp?bassnum = NINC34, accessed on 24/6/2004.
10. Z. JINGCHEN and Y. PING, in Superalloys 718, 625, 706 and Various Derivatives, 2001, edited by E. A. Loria (TMS, Warrendale, PA, 2001) p. 133.

Received 10 March
and accepted 25 June 2004